Original Article

Distribution patterns of landslides triggered by the 2022 Ms 6.8 Luding earthquake, Sichuan, China

ZHANG Jian-qiang[1] https://orcid.org/0000-0003-3908-1082; e-mail: zhangjq@imde.ac.cn

YANG Zong-ji[1] https://orcid.org/0000-0003-4108-2092; e-mail: yzj@imde.ac.cn

MENG Qing-kai[1] https://orcid.org/0000-0002-2019-9702; e-mail:mengqingkai@imde.ac.cn

WANG Jiao[1] https://orcid.org/0000-0001-9300-2280; e-mail:wangjiao@imde.ac.cn

HU Kai-heng[1] https://orcid.org/0000-0001-8114-5743; e-mail:khhu@imde.ac.cn

GE Yong-gang[1]* https://orcid.org/0000-0002-8376-7324; ✉e-mail: gyg@imde.ac.cn

SU Feng-huan[1] https://orcid.org/0000-0002-7355-5715; e-mail:fhsu@imde.ac.cn

ZHAO Bo[1] https://orcid.org/0000-0002-2565-8752; e-mail: zhaobo1989@imde.ac.cn

ZHANG Bo[1] https://orcid.org/0000-0002-7056-1124; e-mail: rsbozh@qq.com

JIANG Ning[1,2] https://orcid.org/0000-0001-8153-3922; e-mail: jiangning@imde.ac.cn

HUANG Yu[1,3] https://orcid.org/0000-0001-6452-7109; e-mail: h.y.mail@qq.com

MING Zai-yang[1,3] https://orcid.org/0000-0003-3431-8378; e-mail: mingzaiyang@163.com

ZHANG Yi-fan[1,2] https://orcid.org/0000-0003-0090-781X; e-mail:zhyf@imde.ac.cn

LIU Zhen-xing[2,4] https://orcid.org/0000-0003-4628-6529; e-mail: liuzhenxing2115@igsnrr.ac.cn

WU Chun-hao[1,2] https://orcid.org/0000-0003-3660-7747; e-mail: wuchunhao@imde.ac.cn

ZHOU Wen-tao[1,2] https://orcid.org/0000-0001-8583-1919; e-mail: zhwt@imde.ac.cn

LIANG Xin-yue[1,2] https://orcid.org/0000-0002-3556-5576; e-mail: liangxinyue17@mails.ucas.edu.cn

SUN Yu-qing[1,2] https://orcid.org/0000-0002-6070-5585; e-mail: sunyuqing@imde.ac.cn

YANG Lian-bing[1,2] https://orcid.org/0000-0003-4250-8761; e-mail: ylb@imde.ac.cn

YAO Hong-kun[1,2] https://orcid.org/0000-0002-9617-5360; e-mail: yhk@imde.ac.cn

FENG Pei-hua[1,5] https://orcid.org/0000-0002-8526-3787; e-mail: 622210960010@mails.cqjtu.edu.cn

LIU Jia-li[1,2] https://orcid.org/0000-0002-4284-2965; e-mail: liujiali@imde.ac.cn

*Corresponding author

1 Institute of Mountain Hazards and Environment, Chinese Academy of Sciences, Chengdu 610041, China

2 University of Chinese Academy of Sciences, Beijing 100049, China

3 East China University of Technology, Nanchang 330013, China

4 Institute of Geographic Sciences and Natural Resources Research, Beijing 100101, China

5 Chongqing Jiaotong University, Chongqing 400074, China

Abstract: At 12:52 pm on September 5, 2022, an Ms 6.8 earthquake occurred in Luding County, Sichuan Province, China. Based on high-resolution aerial photographs and satellite imageries obtained after the

earthquake, as well as field investigation, a total of 8685 earthquake-triggered landslides (EQTLs) were interpreted. The landslides covered an area of 30.7 km², with a source area of 9.4 km². These EQTLs were mainly distributed in areas with a seismic intensity of VIII and IX. Most of the landslides were small and medium in size, and their types included landslide, rockfall, and rock slump. Characteristic landslide distributions were found, EQTLs were distributed along the Xianshuihe fault, landslide area decreased gradually with an increased distance to the fault; EQTLs were distributed along the Daduhe River and roads; besides, landslide distribution was associated with ground deformation caused by the earthquake. EQTLs' characteristics indicated that, a large number of EQTLs were located near the foot of the slope; the full area of EQTLs and their source area followed a power function. This study concluded that Luding EQTLs were greater in number and area but relatively smaller in terms of affected area. Investigations on geo-hazards post-earthquake and risk assessment were proposed in the earthquake-stricken area to support the rehabilitation and reconstruction.

1 Introduction

Earthquakes in mountain areas often trigger large numbers of landslides. Such earthquake-triggered landslides (EQTLs) can bring huge casualties and significant economic losses by blocking rivers and roads and destructing towns and villages, which aggravates the direct damages caused by the earthquake. Additionally, EQTLs could also impede disaster relief efforts by preventing engineering machinery and emergency services from entering the earthquake-stricken area, thus seriously delaying the rescue process (Cui et al. 2008). A few examples include the 1964 earthquake in Niigata, Japan (Ms 7.5), where EQTLs and related soil-liquefaction occurrences caused an estimated US$ 800 million in damage (Lee et al. 1977). The Tecomán earthquake (Ms 7.6) in Mexico in 2003 resulted in a total financial loss exceeding US$88 million where approximately US$6 million were attributed to landslide-caused highway damage (Keefer et al. 2006). Therefore, it is important to investigate and analyze EQTLs' characteristics and distribution

patterns, which underlies the basis for EQTL risk assessment, as well as post-earthquake hazards assessment and reconstruction.

Methodologies for EQTL investigation and inventory include field investigation, papery aerial imagery-based interpretation, visual interpretation based on digital remote sensing imagery, as well as automatic interpretation (Xu 2012). Presently visual interpretation combined with field investigation is commonly used. By using the above methods, scholars worldwide have built EQTL inventories for single or multiple earthquake events and conducted analyses of distribution patterns of EQTLs. For example, Keefer (1984) and Rodríguez et al. (1999) collected and established landslide inventories for 36 earthquake events worldwide from 1811 to 1997, and analyzed the relationship of earthquake magnitude with landslide number, area, landslide-affected area, and maximum distance from the seismogenic fault. A large number of studies were concentrated on a single earthquake event. Examples include landslides induced by the 1994 M_S 6.7 Northridge earthquake, California, USA (Jibson and Harp 1994; Harp and Jibson 1996), 1999 ChiChi Earthquake, Taiwan, China (Wang et al. 2003), 2008 M_S 8.0 Wenchuan earthquake (Dai et al., 2011; Xu et al. 2012), 2010 M_S 7.1 Yushu earthquake (Xu et al. 2012), 2013 M_S 7.0 Lushan earthquake (Su et al. 2013; Zhang et al. 2013; Cui et al. 2014), 2015 M_S 7.8 Nepal Gorkha earthquake (Regmi et al. 2016; Roback et al. 2018), and 2017 M_S 7.0 Jiuzhaigou earthquake (Ling et al. 2021). Based on EQTL inventories, numerous studies that have been conducted focus on the spatial distribution patterns and characteristics of EQTLs. All EQTL events tended to have significant spatial distribution features. For example, EQTLs decrease gradually with increasing distance to the seismogenic fault or epicenter, landslides are closely related to peak ground acceleration, and the hanging wall/footwall effect exists for landslides triggered by thrust fault earthquakes. EQTLs are fairly correlated with stratigraphic lithology. For instance, the proportion of rockfalls is mainly distributed in hard rocks zone in the Wenchuan earthquake. In addition, EQTLs also have connections with topographic factors such as slope degree, elevation, curvature, and slope aspect (Wang et al. 2003; Qi et al. 2010; Dai et al. 2011; Roback et al. 2018; Zhuang et al. 2018; Zhao 2021).

At 12:52 pm on September 5, 2022, an M_S 6.8

earthquake (China Earthquake Administration) happened in Luding County, Ganzi Prefecture, Sichuan Province, China. The epicenter of the earthquake was located at 29.59° N, 102.08° E, and the focal depth was 16km. The earthquake triggered a large number of landslides, which caused significant damages to urban buildings, transportation, telecommunication, power lines, and other facilities. The highest intensity of the Luding earthquake reached IX. The area with earthquake intensity of VI and above was more than 19,000 km². After the earthquake, Chinese scholars investigated EQTLs and conducted preliminary analyses based on obtained landslide data. Fan et al. (2022) interpreted 3,633 landslides triggered by the Luding earthquake with a total area of 13.78km², while Tie et al. (2022) mainly focused on EQTLs that were threatening to communities. A total of 565 hazard points were interpreted and identified, including 331 rockfalls and 234 landslides. Because these works were based on emergency investigation, EQTL inventory was not complete due to limited remote sensing imageries.

In this study, high-resolution aerial photographs and satellite images before and post the earthquake were utilized, with field investigation and validation being carried out simultaneously. A detailed landslide inventory was established. Spatial distributions and characteristics of Luding EQTLs were analyzed based on the landslide inventory.

2 Study Area

The Luding earthquake-stricken area was located in the western mountainous area of Sichuan Province, China (Fig. 1A). In this research, study area included the areas of Luding earthquake with an intensity of VIII and IX, and partial areas with an intensity of VII.

2.1 Geological setting

The seismogenic fault of the Luding earthquake is Xianshuihe Fault, which is a large sinistral strike-slip fault that stretches for about 350km (Wu et al. 2016). The epicenter of Luding earthquake is located on the Moxi fault in the southeastern portion of the Xianshuihe Fault (Fig. 1B).

In terms of stratigraphic division, the study area belongs to the South China stratigraphic region. To the east of the Xianshuihe fault, a set of Paleozoic Marine and Mesozoic continental strata, basic-ultrabasic rocks, diorites and granites were mainly
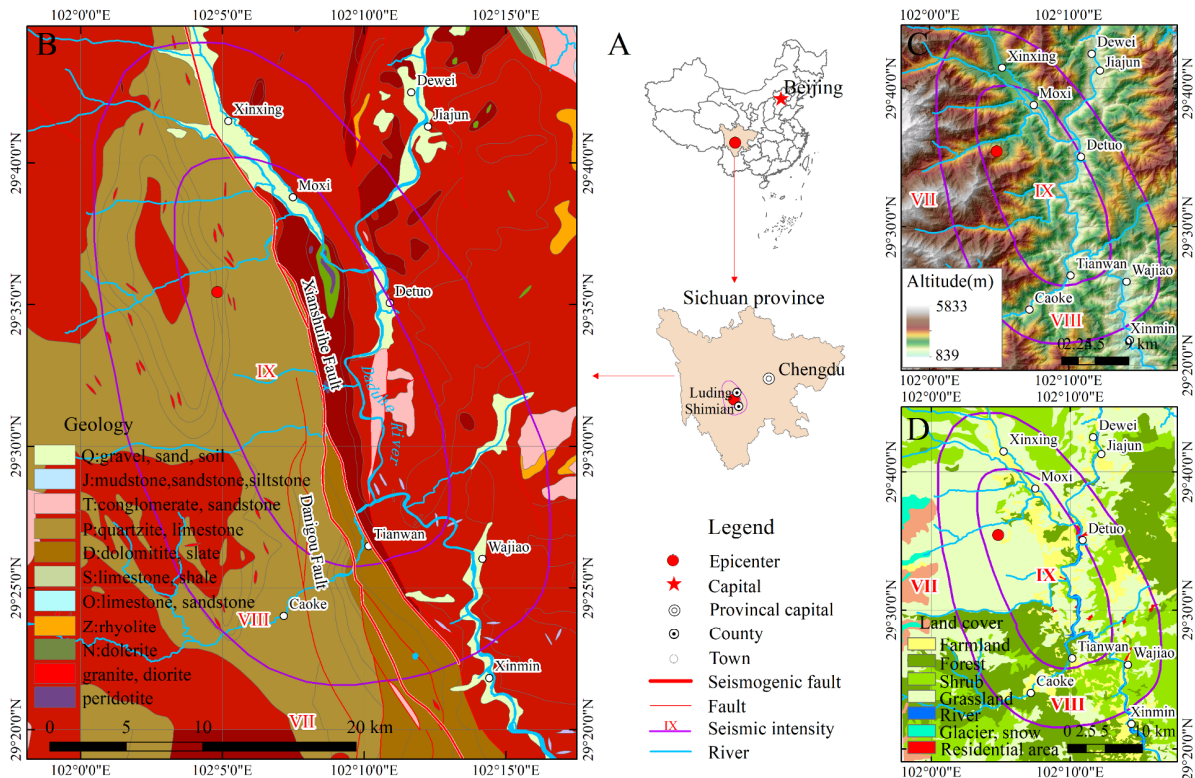
Fig. 1 Study area. (A) Location of study area; (B) Geological map; (C) Topographical map; (D) Land cover map.

distributed. Quaternary strata are scattered in ancient planation surface, intermountain basins, and river valleys. Intrusive rocks are largely distributed to the east of the Danigou fault. Intrusive rocks are mainly granite, monzonite, and diorite. In the east of the Danigou fault, basic Dikes and acid Dikes are also distributed where the basic Dikes are mainly diabase and allgovite.

2.2 Geomorphological setting

The Luding earthquake-stricken area is located in the middle of the high mountains of southwest Sichuan, which is a transitioning area from the southeastern margin of the Tibet Plateau to the Sichuan Basin (Fig. 1C). The study area is characterized by high mountains and deep-cutting valleys where the west and north sides have a higher altitude than the east and south, respectively. For example, Gongga Mountain peak with an altitude of 7556m is located in the west, while Ma'an Mountain and Huangcao Mountain with an altitude of 4021m and 3661m, respectively, are both located in the east. The main ranges run south to north, which are controlled by a large scale tectonic line.

2.3 Land cover types

The vegetation in the study area is well developed as shown in Fig. 1D. Areas of grasslands, forests, and shrubs are very large in this area, accounting for 39.8%, 24.2% and 22.6%, respectively. Due to considerable elevation differences in the study area, the vegetation shows a characteristic of a vertical spectrum with land cover types of forests, shrubs, grassland, and bared rock from the valley to the top of the hill. Rich vegetation in the study area is conductive to EQTL interpretation by comparing the pre- and post- earthquake land cover changes.

3 Methodology and Data Sources

3.1 EQTL investigation

Aerial photographs and high-resolution satellite imageries were the main data sources for landslide interpretation (Table 1). The investigation covered a total area of 19,000km², including 160km² captured by aerial photographs, and another 18840km² by

Table 1 Remote sensing imageries used for Luding EQTLs interpretation

Period	Type	Resolution (m)	Acquisition time
Pre-earthquake	ZY-1	2.36	2022.07.08
	Sentinel-2	10	2021.04.29
Post-earthquake	Aerial images	0.2	2022.09.06 -2022.09.10
	BJ3A	0.5	2022.09.10
	GF-6	2	2022.09.10

satellite images such as BJ-3A and GF-6 images (Fig. 2). Among them, aerial photographs had the advantages of high resolution (0.2m) and less cloud covering, but its coverage area was relatively limited. Aerial photographs were mainly striped along roads and river valleys, which were just a small part of the whole earthquake-stricken area. Thus the area not covered by aerial photographs was supplemented by BJ-3A and GF-6 satellite imageries. BJ-3A remote sensing imageries had a resolution of 0.5m, which mainly covered the epicenter area. GF-6 remote sensing imageries had a lower resolution of 2m but covered the largest area. These three imageries were utilized together to achieve the full coverage of the earthquake-stricken area.

The visual interpretation method was utilized for landslide interpretation. The method was known for higher precision than automatic landslide extraction. Prior to interpretation, remote sensing imageries were first enhanced by pansharpening and geometric rectification (Guzzetti et al. 2012; Zhong et al. 2020). EQTL interpretation standard criteria summarized by Fan et al. (2019) were followed in this research. Remote sensing imageries covered the whole area affected by the earthquake, and all identified EQTLs were mapped. Landslide boundaries, as well as landslide source area boundaries were mapped rather than landslide point locations. Complex landslides with joint boundaries were separated into different individual landslides based on their topographic features. And landslides were mapped in a shape layer with a projected coordinated system.

Besides, field investigation is a very essential way that supplies validation and more information complement to remote sensing interpretation. A field investigation on Luding EQTLs was carried out simultaneously from Luding County to Shimian County (Fig. 2A), including Moxi town near the epicenter area. The main tasks of the field investigation included validations of landslide location and boundary, as well as identification of
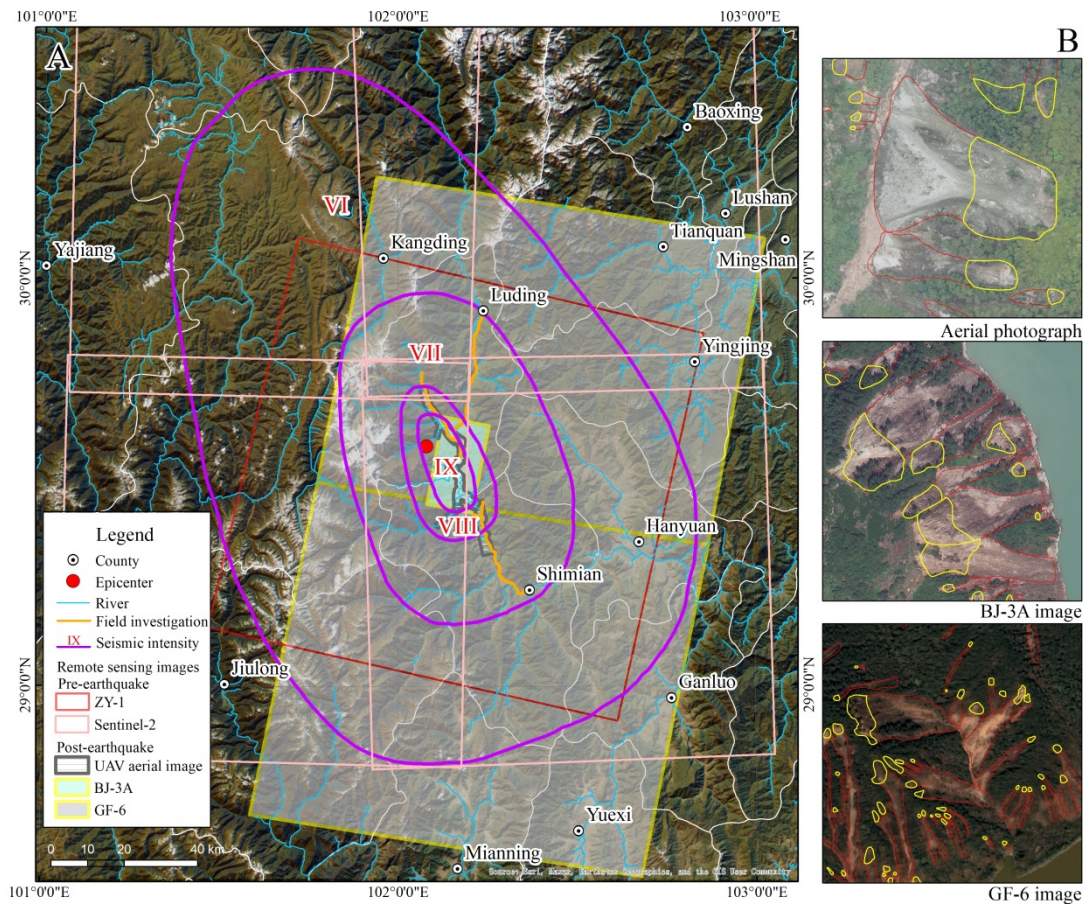
Fig. 2 Earthquake-triggered landslide (EQTL) interpretation. (A) Coverage of pre- and post-earthquake remote sensing imageries; (B) Examples of different types of remote sensing imageries used for EQTL interpretation. Source (yellow) and full area (red) boundaries of each EQTL are differentiated.

landslide types, and geologic and topographic features.

3.2 Data sources

The topographic data used in the research was based on ALOS PALSAR DEM with a spatial resolution of 12.5m. For geological and fault data was obtained from China national digital geological map spatial database (public version at 1:200000 scale) (Li et al. 2019). Land use datasets were provided by the Resource and Environment Science Data Center of the Chinese Academy of Sciences (RESDC) (Xu et al. 2018). And seismic data were obtained from the China Earthquake Administration.

4 Distribution Patterns of Luding EQTLs

4.1 Landslide inventory

Luding EQTL inventory (Appendix 1) was established with a total of 8685 landslides interpreted (Fig. 3). The landslides covered an area of 30.7km², with a source area of 9.4km². Landslide-affected areas were about 760km². The number of landslides with an earthquake intensity of VII, VIII and IX was 443, 2452 and 5790, respectively. Statistics of the landslides show that EQTLs in the study area were mainly small or medium-sized. There were 47 landslides with an area range of 50,000-100,000 m². In addition, only 20 landslides occurred larger than 100,000 m² (Table 2).

4.2 Types of EQTLs

Dynamic characteristics and movement processes are the main principles for classifying the types of landslides (Varnes 1954; Varnes 1978; Hungr et al. 2014). According to the classification principle of landslides, there were three main types of EQTLs: slide, rockfall and slump were found in Luding
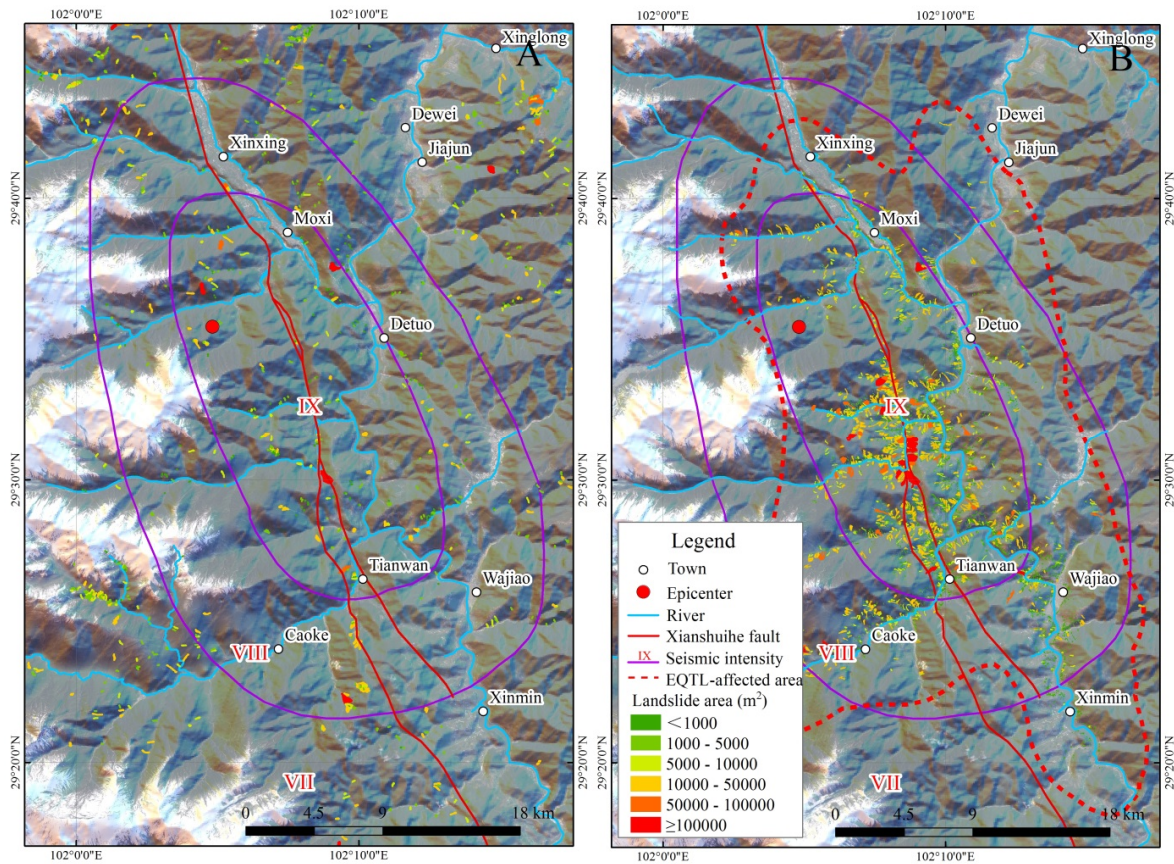
Fig. 3 Distribution of landslide in Luding earthquake-stricken area. (A) Landslides before the earthquake; (B) Earthquake-triggered landslides.

Table 2 Statistics of Luding earthquake-triggered landslide area

Earthquake intensity	Landslide area (m²)						Total
	< 1000	1000-5000	5000-10000	10000-50000	50000-10000	≥100000	
VII	325	48	24	42	3	1	443
VIII	1515	638	160	127	7	5	2452
IX	3055	1796	439	449	37	14	5790
Total	4895	2482	623	618	47	20	8685

earthquake-stricken area. These different types of landslides were characterized as follows: landslides' movement was along a defined sliding surface; rockfalls were the movement of rock and soil mass along steep slope by rolling, jumping, or falling without terrain constraints; slumps had a clear top scarp and a fixed sliding surface, and often occur in a very steep slope. Therefore, the movement of slumps has both characteristics of landslides and rockfalls. Features of different types of EQTLs could be reflected from the typical landslide sites as flow.

4.2.1 Aiguo Village landslide group

The landslide group was located on the slope of the riverbank near Aiguo Village, Wanggangping Town, Shimian County, with the longitude and latitude coordinates of 102°09'45"E, 29°26'38"N. The Aiguo Village landslides were 10km away from the upper reach of Dagangshan Hydropower Station. The landslides were deformed due to the impoundment of hydropower station in history. The volume of the landslides was in the millions of cubic meters. This section of the river where the landslide located was straight and oriented nearly in the north-south direction. The river valley was V-shaped. The slope of the left bank was slightly slower, with an average slope degree of about 40°. The top elevation of the slope was about 1300 m, where there were some
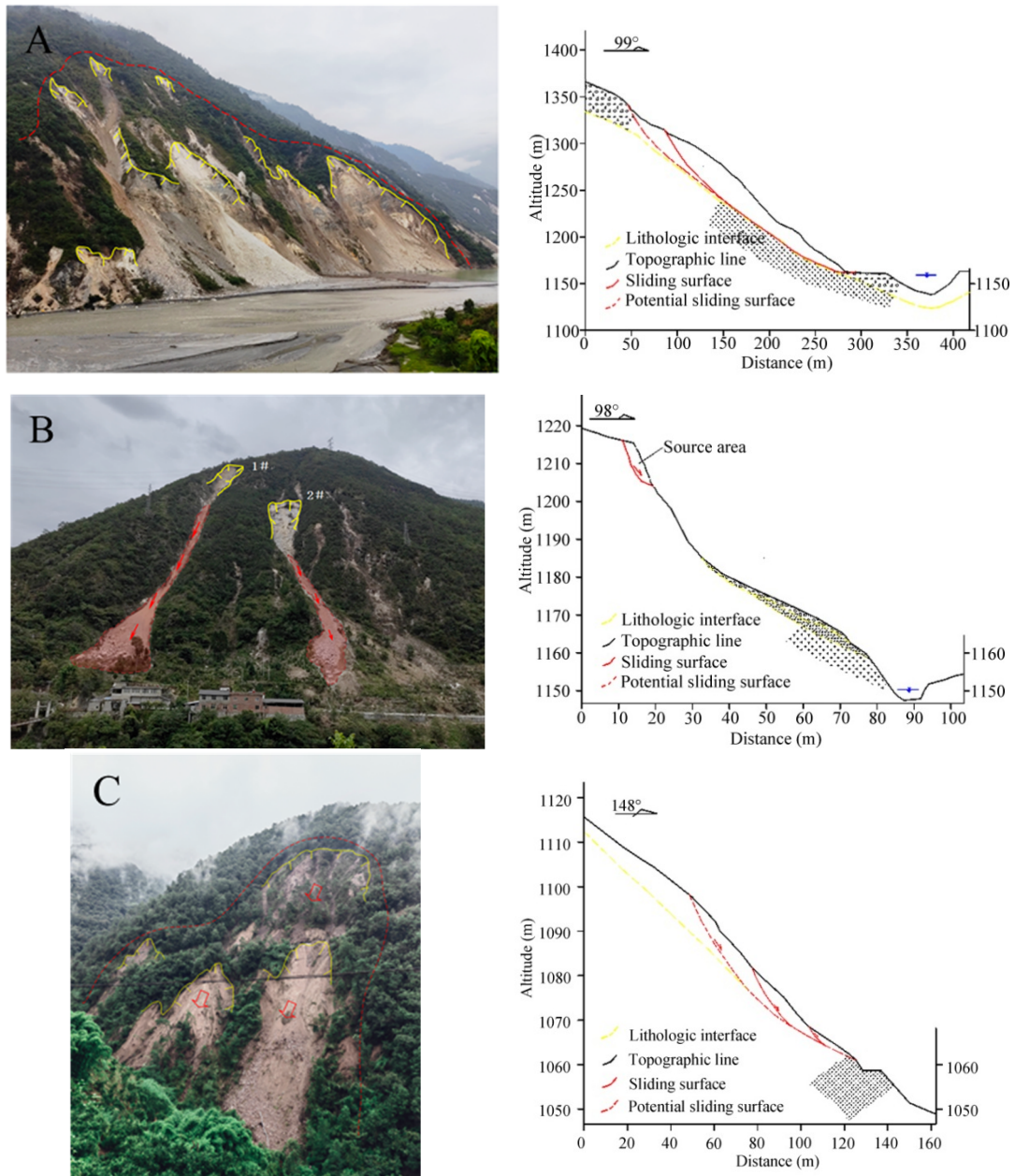
Fig. 4 Different types of landslide triggered by the Luding earthquake. (A) Aiguo Village landslide group; (B) Xiakuiwu Village rockfall; (C) Xiaoma Village slump. (Landslide profiles were supplied by ZHU Lei).

settlements and cultivated land distributed. Vegetation on the slope was good, with shrubs on the steep slope and trees on the top. The bedrock of the slope was granite.

The topography of Aiguo village landslides presented a typical arm-chair shape (Fig. 4A). The width of landslides toe along the river was about 400m, with a runout length of about 200m. The slope gradient of main scarp, the middle part and toe of landslides were 45°, 47°, 65° respectively, and the main sliding direction was 99°. The size of landslides

was $8.0 \times 10^4 m^2$ in area and about $2.4 \times 10^5 m^3$ in volume. The altitudes of the landslide toe and back scarp were 1150m and 1370m, respectively, and the relative relief was 220m. The depth of the landslide was about 15~30m.

4.2.2 Xiakuiwu Village rockfall

The rockfall was located in XiaKuiwu Village, Detuo Town, Luding County, on the right bank of Daduhe River, with the latitude and longitude coordinates of 29°36 '43" N, 102°09' 72" E. The banks

on both sides of the Daduhe River were steep in a U-shaped valley (Fig. 4B).

The altitude of the top of the slope where Xiakuiwu Village rockfall located was about 1400m, with an average slope gradient of about 30°-50°. Before the rockfall occurred, the surface of the slope was well covered by vegetation. The material of the slope foot was dense quaternary residual deluvium mainly a composite of gravel soil. Particle size of the stones was 0.3-1m. The bedrock of granite was moderately - strongly weathered with a blocky structure.

The Luding earthquake loosened the top part of the slope, causing the deluvium and rock mass to slide in a long distance along the channel. The bedrock was weak to strong weathered, with a blocky and sub-blocky structure. The accumulation area of the rockfall was about 60m in width, and 180m in length. Granite blocks with diameters of 5m, 1-5m, and smaller than 1m were account for 20%, 70%, and 10% respectively. Due to the high position of the source area, the rockfall body was further broken during the movement, and turned into clastic flow to accumulate at foot of the slope.

4.2.3 Xiaoma Village slump

The Xiaoma Village landslide was a typical earthquake-triggered slump. The slump was located near Xiaoma Village, Wanggangping Town, Shimian County, with the latitude and longitude of 102°13'22" N, 29°23'49" E. The toe of the slump was located on the lower side of the road at an altitude of 1,050m. The altitude of the main scarp was 1,140m to 1,150m, with an altitude relief of about 90-100m.

The slump was horseshoe shaped, with a main sliding direction of 140°-150°. The width was about 50-85m, and the length was about 200m. The area of the slump was about 16,000 m², with the thickness of 2-5m. The volume of the slump was about 80,000m³. The slope gradient of the slump was 45°-50°, and the top was slightly gentler with slope gradient of 20°-25°. The deluvium on the slope was composite of gravel soil with loose to slight dense structure (Fig. 4C). The slump was located near the ridge of a huge and gentle southern slope. Based on the field measurement, height of the main scarp, the secondary scarps of the left and right parts were 20-40cm, 1.7-2.5m and 3.2-5.4m, respectively. The road that crossed the slump body had obvious signs of subsidence and rupture. As bedrocks could be seen at the top of the slope, therefore the slump would not continue to be enlarged upward.

4.3 Spatial distribution of EQTLs

#### 4.3.1 Distribution along active faults

The most significant spatial distribution characteristics of EQTLs were reflected by their relationship with epicenter or seismogenic fault (Fig. 5A). Statistics on EQTLs area and the distance to epicenter showed that, there was a tendency for the landslide area to decrease gradually with the distance from the epicenter overall (Fig. 5B), but the area of seismic landslides within 5km of the epicenter was not the highest. On the one hand, because the seismic energy release was mainly transferred from the seismogenic rupture to both sides, resulting surface damage was mainly distributed along the fault, which can also be seen from the seismic intensity map, and thus the place where EQTLs was very serious may not be at the epicenter area. On the other hand, the area of 5 km from the epicenter was small, and the area of EQTLs was also relatively small. Area of the EQTLs showed a tendency of exponential decline with increased distance to the Xianshuihe fault, where a correlation followed the relationship of $y = 51.023e^{-0.866x}$ (R^2=0.8821). EQTLs were mainly concentrated within 2km from the fault, accounting for 51.7% of the total landslide area (Fig. 5C). On both east and west sides of the Xianshuihe fault, the landslide area decreased as the distance from the fault increased. The largest landslide area was within 2 km of the east side of the fault, accounting for 28.3% of the total landslide area; in the range of 0-2km and 2-4km, landslide area on the east side of the fault was larger than that on the west side (Fig. 5D).

The density of EQTLs along the Xianshuihe fault was analyzed (Fig. 6A, 6B). Three peak values of landslide density were identified in the fault from south to north. They were located in the Yanzigou (the epicenter), Dagou and Tianwan River basins, respectively, where the latter two had a relatively higher landslide density.

4.3.2 Distribution along the river

Luding EQTLs were spatially distributed along rivers, especially the Daduhe River (Fig. 7B, 7C, 7D). In the study area, the Daduhe River flows from north to south, basically parallel to the Xianshuihe fault. A total of 4160 EQTLs were distributed within 1km to
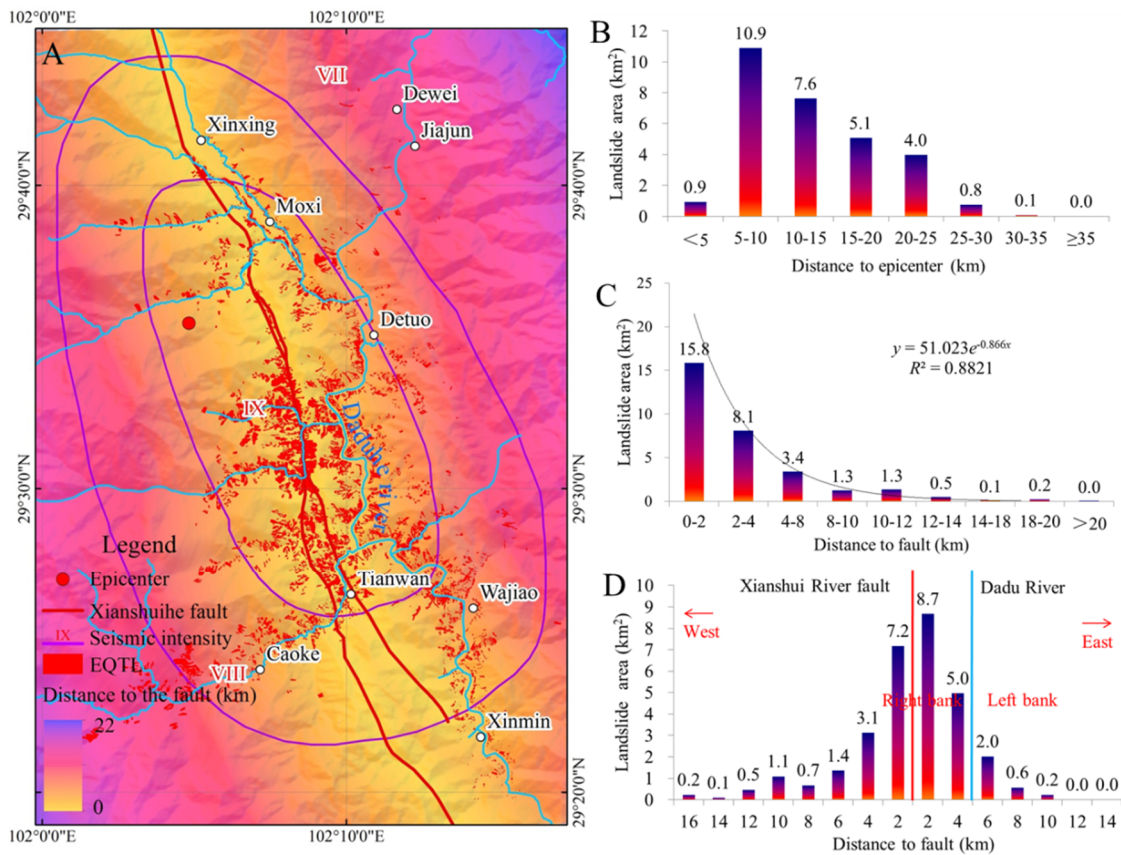
Fig. 5 Earthquake-triggered landslides (EQTLs) along the Xianshuihe fault. (A) Landslide distribution map to show the distance to the fault; (B) EQTLs distribution at different distances from the epicenter; (C) EQTLs distribution at different distances from the Xianshuihe fault; (D) EQTLs distribution on both sides of the Xianshuihe fault.

the Daduhe River in an area of 91.7km², accounting for 47.9% of the total number of landslides, and the landslide covered 8.4% of the area. Likewise, EQTLs occurred along some rivers perpendicular to Xianshuihe fault. Take Dawangou River as an example (Fig. 7A), there were 876 EQTLs were distributed within the 10km length and an area of 16.5 km² along the river, and the landslides covered 10.4% of the area.
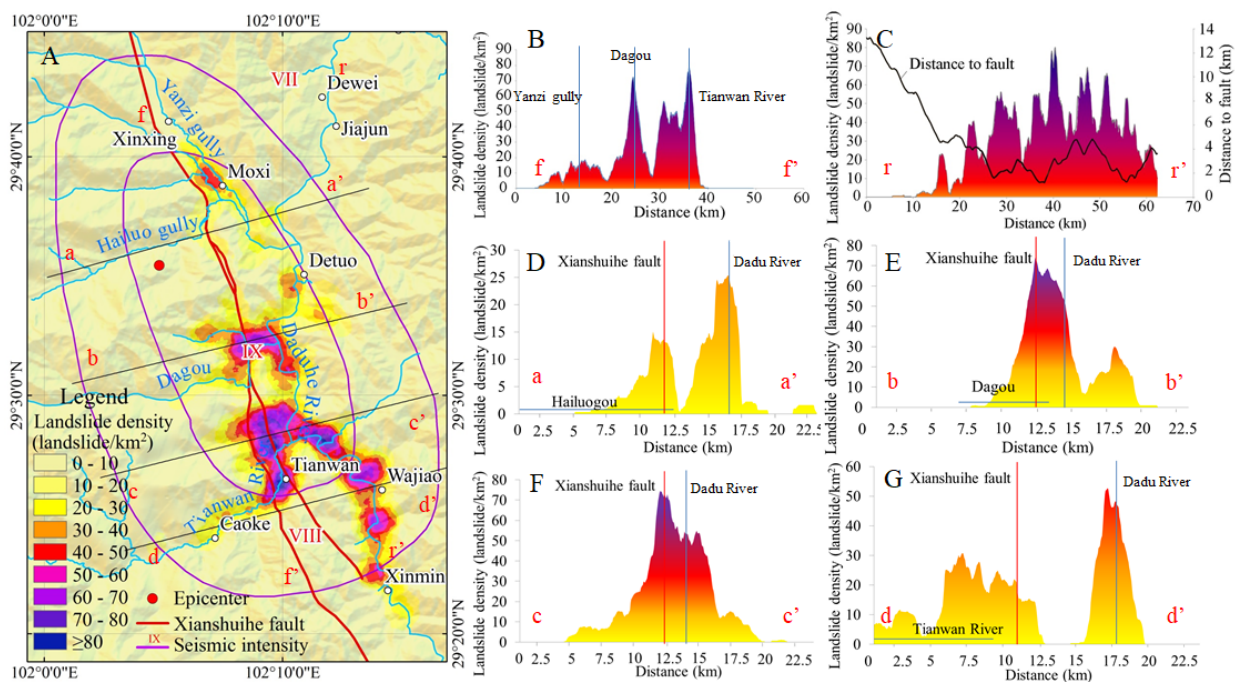
The density of landslides along the Daduhe River in the earthquake-stricken area was relatively high (Fig. 6C). The density profile showed that, the density from Maituo Town to Xinmin Town was mostly higher than 30 landslides per square kilometer, partly because this section of Daduhe River was very close to the Xianshuihe fault, with a distance basically less than 4km. Moreover, due to the downcutting of the river, both sides of river bank were characterized by steep slope, where were prone to EQTLs.

Four landslide density profiles perpendicular to the Xianshuihe fault were drawn, which showed areas

near the Xianshuihe fault and Daduhe River had a high density of landslides. Two profiles in the middle of the study area showed areas near the Xianshuihe fault had the highest landslide density (Fig. 6E, 6F). But for the profiles on the northern and southern sides, the highest landslide density appeared near the Daduhe River, even greater than the density near the Xianshuihe fault (Fig. 6D, 6G).

4.3.3 Distribution along the road

Distributing along the road was also one prominent distribution feature for Luding EQTLs. An example was one section of road connecting Detuo town to Daba villiage in the area with an earthquake intensity of IX (Fig.8A). The road with a length of 3.9 km was built on the right bank of the Daduhe River and on the west side of the Xianshuihe fault. 145 EQTLs were distributed along the road with an area of 0.3km². These landslides caused about 2.0 km of road damage with a ratio of 51.3%. Another example was a section of the 5.3km road (Fig.8B) located to the

Fig. 6 Density characteristics of Luding earthquake-triggered landslides (EQTLs). (A) Density map of the landslides; (B) Landslide density profile of ff' along the Xianshuihe fault; (C) Landslide density profile of rr' along the Daduhe River; (D) Landslide density profile of aa'; (E) landslide density profile of bb'; (F) landslide density profile of cc'; (G) landslide density profile of dd'.
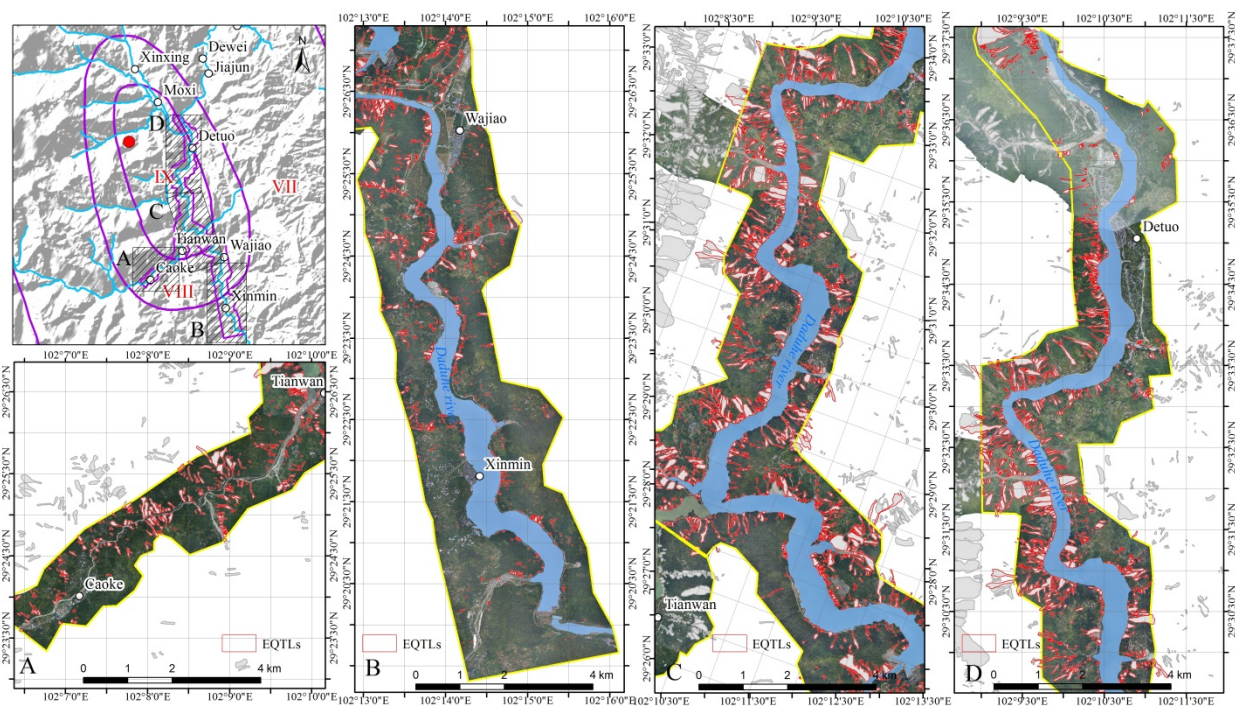
Fig. 7 Distribution of the Luding earthquake-triggered landslides along the Daduhe River.

northwest of Wajiao Town with an earthquake intensity of VIII. 107 EQTLs with an area about 0.1km² occurred along the road, which blocked or damaged 3.2km of the road, and the damage proportion reached 60.4%. On the one hand, since roads were mostly built at the foot of slopes and along rivers or valleys, therefore, these areas were prone to the EQTLs. On the other hand, topography was
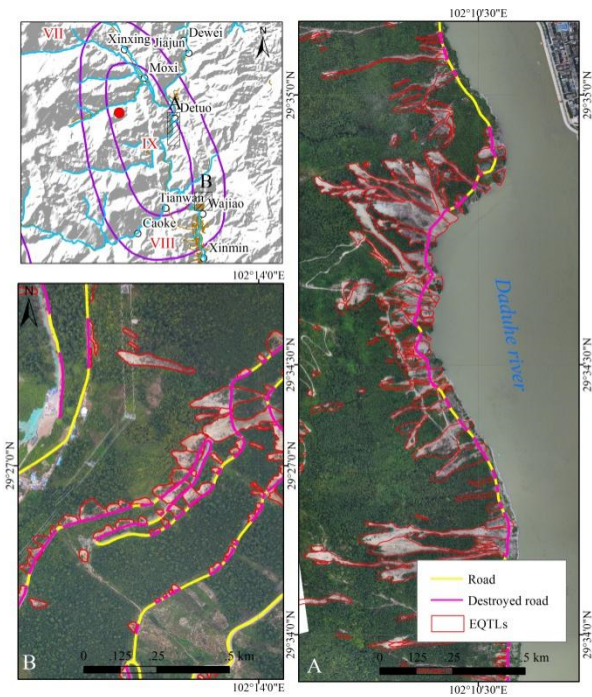
Fig. 8 Earthquake-triggered landslides distributed along the road.

Fig. 9 Distribution of surface deformation caused by the Luding earthquake.

changed and high and steep slopes formed during the construction of the road, which was easy to collapse under the impact of earthquake.

4.3.4 EQTLs with surface deformation

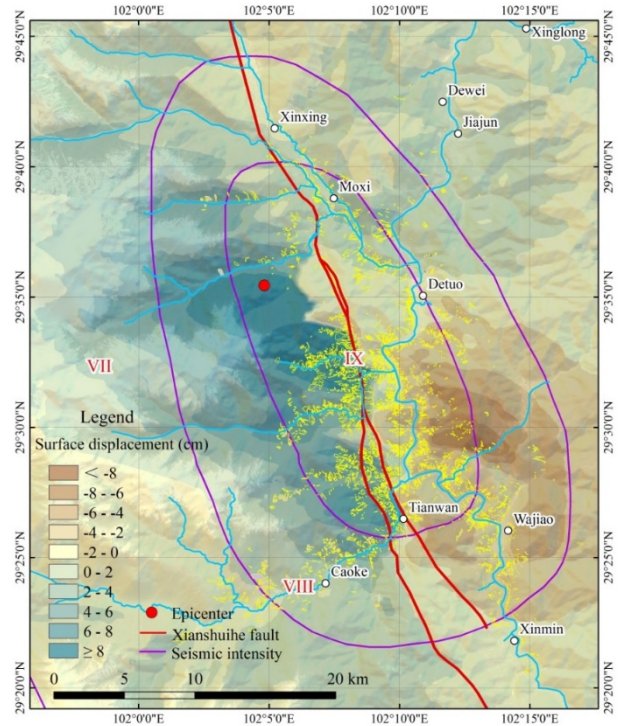The pre- and post-earthquake descending orbit Sentinel-1 SAR images (acquired on September 2, 2022 and September 14, 2022, respectively) were used for differential interference processing and calculating surface deformation in the earthquake-stricken area (Fig. 9). The positive value was near the LOS direction (westward direction) while the negative value was away from the LOS direction (eastward direction).

The surface deformation calculated by SAR images showed that the east side of the Xianshuihe fault mainly exhibited an eastward deformation, while the west side mainly exhibited a westward deformation. The surface deformation accorded with the characteristics of a sinistral strike-slip fault. Statistical analyses of EQTLs and surface deformation showed that, Luding EQTLs were mainly distributed in the junction area of different deformation directions. A large number of EQTLs were distributed in the area of westward deformation, especially in areas with surface deformation of 0-2cm, and 4-6 cm.

Note that for the area with deformation of 0-2cm, the real deformation may exceed the detecting ability of D-InSAR.

5 Characteristics of Luding EQTLs

5.1 Positions on the slope

Three parameters were proposed to describe the position of EQTLs on the slope (Meunier et al. 2008): (1) distance from landslide scarp to the crest ridge; (2) distance from the landslide toe to the slope foot; (3) the length of the slope where landslides were located. Then, the distances from the landslides to the ridge and the slope foot were normalized.

$$\left| d_{st,top} \right| = \frac{d_{st,top}}{d_{st} + d_{top}} \tag{1}$$

The $|d_{st}|$ was the normalized distance from the landslide toe to the slope foot, and $|d_{top}|$ was the normalized distance from landslide scarp to the crest ridge. The plot figure was drawn based on both normalized values, which indicated the relative position of EQTLs on the slope. $|d_{top}|$ was utilized to
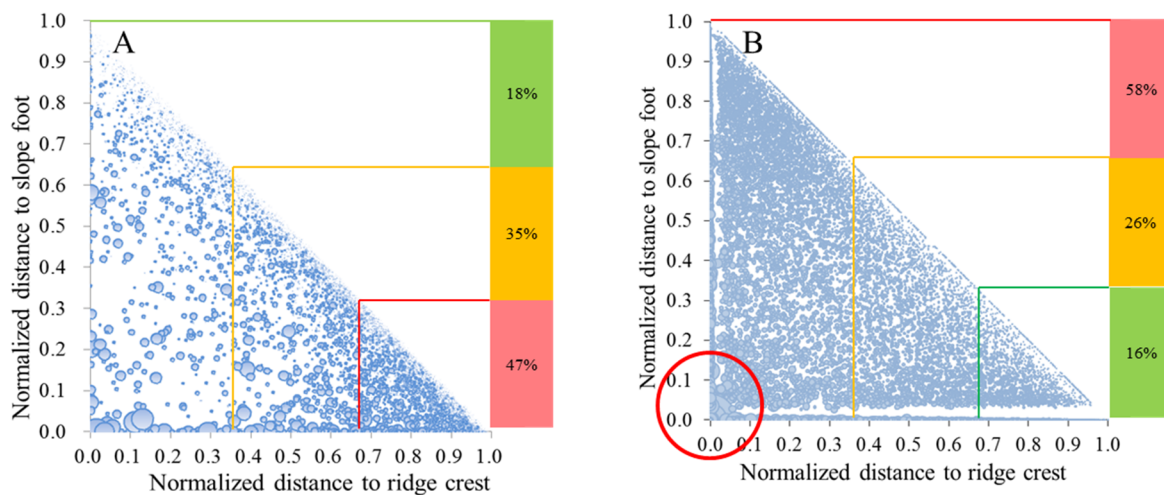
Fig. 10 Relative position of earthquake-triggered landslides (EQTLs) with respect to ridge crest and slope foot. (A) Luding EQTLs; (B) 2008 Wenchuan EQTLs. The red circle shows that, numerous large size landslides occurred on the ridge crest and moved to the slope foot during the 2008 Wenchuan earthquake.

describe and count the relative position where landslides occur. If $|d_{top}|$ was equal to 0, the EQTL occurred on top of the slope. If the $|d_{top}|$ value was equal or close to 1, it meant the EQTL occurred in the slope toe.

Statistical results showed that a large proportion of Luding EQTLs was located near the foot of the slope, accounting for 47% of the total landslides, while landslides located near the ridge of the slope accounted for only 28% (Fig. 10A). Different from Luding EQTLs, landslides induced by the Wenchuan earthquake were mainly located in the area near the ridge, accounting for 58% of the total landslides, while the landslides near the foot of the slope accounted for only 16% (Fig. 10B). In addition, when considering other EQTLs worldwide, 56% of the landslides induced by the Northridge earthquake (17 January 1994, Ms 6.7) were located near the mountain ridges; the landslides induced by the two earthquakes (Ms 6.7 and 6.9) in 1993 in the Finisterre mountains were of a bimodal type, with about 33% of the landslides located near the crest ridge and 29% near the foot of the slope (Meunier et al. 2008).

Many large-sized landslides occurred from the top of the slope body and accumulated at the foot of the slope. In the slope position map, these landslides were located at the origin. Since the Wenchuan earthquake induced a large number of large landslides, so there were many landslide circles located at the origin (Fig. 10B). In contrast, there were far fewer such large landslides induced by the Luding earthquake.

5.2 Source area

In addition to the boundary of Luding EQTLs, source area was also identified during the landslide investigation. Statistic results showed that there was a power function relationship between the source area and the total area of the landslides (Fig. 11A). Similar characteristics were found in Gorkha EQTLs in Nepal in 2015 (Roback et al. 2018). However, compared with Gorkha EQTLs with silmilar area, the source areas of Luding EQTLs were larger. A scatter plot was drawn to analyze the correlation of the mean slope gradient of landslide source area with landslide source area/full area ratio. The ratio of source area was mostly concentrated between 20% and 60%, while the mean slope gradient of source area was mainly between 30° and 50°. However, the two parameters did not correlate well (Fig. 11B).

5.3 Runout length

Horizontal runout length could characterize the movement and damaging range of the landslides. Many scholars have carried out analyses on the relationship between the horizontal runout length of EQTLs and related parameters (Yang et al. 2013; Guo et al. 2014; Roback et al. 2018). In this study, the frequency of different runout length was analyzed at first, and their curve showed similar features with the frequency-area curve (Fig. 12A). EQTLs with a runout length less than 40m accounted for 42.8% of the total number of landslides, among which landslides with a
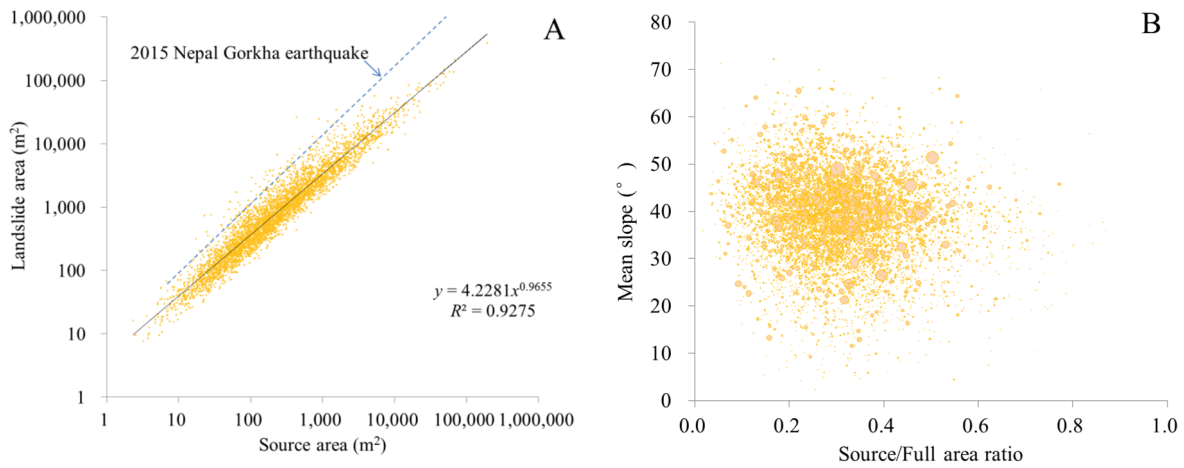
Fig. 11 Source area of landslides triggered by the Luding earthquake. (A) Correlation between landslide source area and landslide area; (B) Correlation between mean slope and source area/full area ratio.
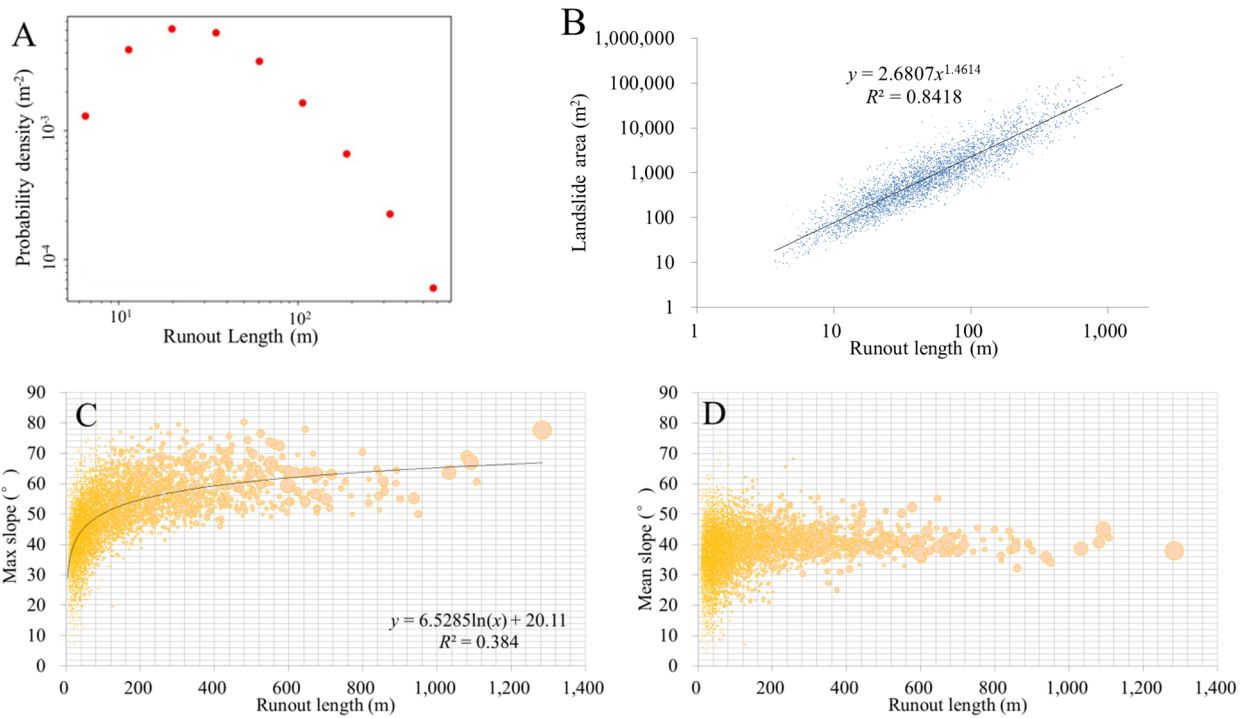
Fig. 12 Characteristics of earthquake-triggered landslide runout length. (A) Frequency-runout length curve; (B) Correlation between landslide area and runout length; (C) Correlation between the maximum slope and runout length; (D) Correlation between the mean slope and runout length.

runout length of 20-30m and 10-20m accounted for the most, and both of them reached 14.1%. Generally speaking, the size of the landslide determined its runout length. The larger the landslide size was, the farther the runout length would be. Landslide area could be used to represent the size of the landslide. Statistical results showed a good power function relationship between EQTL area and runout lengths (Fig. 12B). There was a weak logarithmic correlation

between the maximum gradient with the runout length, though. The overall tendency indicated the larger the maximum slope of the landslide, the farther the runout length (Fig. 12C). However, there was no functional correlation between the mean slope and the runout length. Landslides with a large runout length mainly had a mean slope of 30-50 degrees. Both plots suggested the size of landslides played a more significant role in the runout length (Fig. 12D).

6 Discussions

6.1 Comparison with other EQTL events

6.1.1 Total quantity and area of EQTLs

Based on the worldwide EQTLs inventories collected by Xu (2012), as well as the M_S 7.0 Lushan earthquake in 2013 (Su et al. 2013) and the M_S 7.0 Jiuzhaigou earthquake in 2017 (Ling et al. 2021) occurred in China in recent years, the relationship of the earthquake magnitude with the number and area of landslides was analyzed. Compared with the EQTLs worldwide, the number of landslides triggered by the Luding earthquake was larger than those by the Yushu earthquake (M_S 7.1), Lushan earthquake and Jiuzhaigou earthquake in China, but slightly smaller than the Northridge earthquake (M_S 6.8) in the United States (Fig. 13A). In terms of the total areas, Luding EQTLs had a larger area than the ones by the Yushu earthquake, Lushan earthquake, and Jiuzhaigou earthquake. Although the number of landslides induced by the Northridge earthquake was slightly higher than those by the Luding earthquake, the area of Northridge EQTLs was smaller (Fig. 13B).
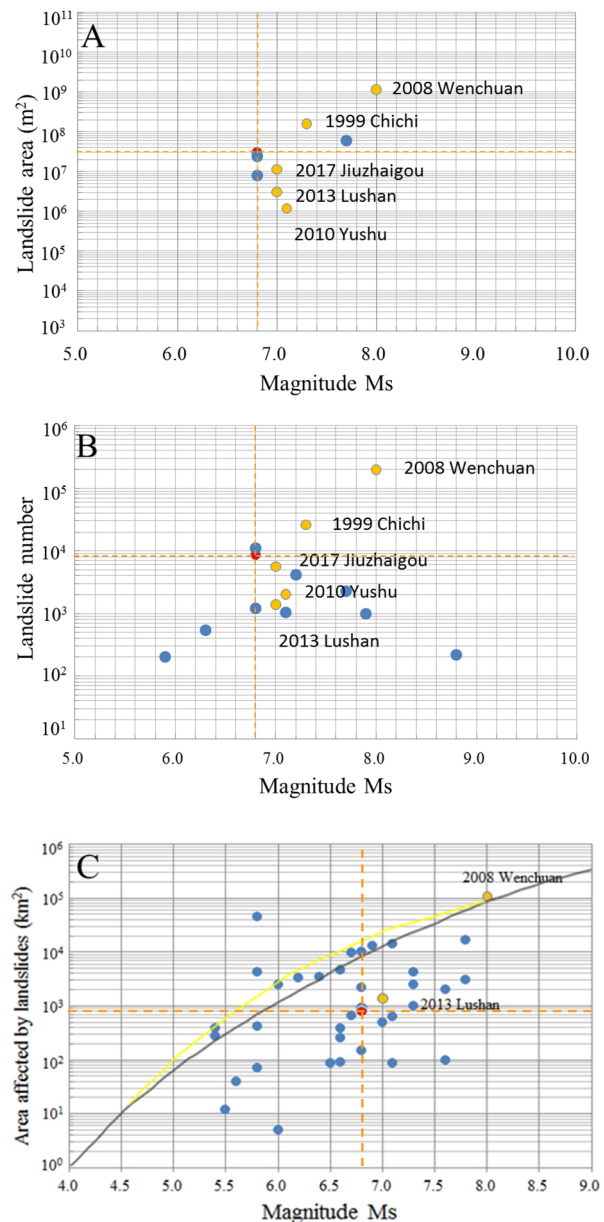
6.1.2 Landslide affected area

The landslide-affected area is another parameter to describe the overall extent of EQTLs. It can also characterize the magnitude of impacts by EQTLs. Luding EQTL-affected area was compared to other 38 EQTL events, which including 36 events produced by Rodríguez et al. (1999), as well as that of Wenchuan EQTLs (Xu 2012) and Lushan EQTLs (Fig. 13C). Statistical results showed that landslide-affected area of the Wenchuan earthquake was located above the upper envelope line, indicating that Wenchuan EQTL-affected area exceeded the average of the global earthquake-triggered landslide events. But the Luding EQTL-affected area was located below the lower envelope, which indicating that the landslide-affected area was fairly smaller compared to other earthquake events with similar magnitude.

Hence Luding EQTLs could be characterized by a large number, a large overall area, and a relatively concentrated distribution in this region.

6.1.3 Size of EQTLs

The landslide area-frequency curve shows the proportional characteristics of landslides of different sizes. It can also reflect the overall magnitude of

Fig. 13 Statistics on (A) landslide number, (B) landslide area and (C) landslide-affected area by earthquake magnitude Ms. Yellow line is the upper bound determined by Keefer (1984), and black line is the new upper bound line proposed by Rodríguez et al. (1999). Red dot: Luding earthquake; Orange dot: earthquakes in China; Blue dot: earthquakes outside of China.

EQTL event (Malamud et al. 2004). m_L is used to characterize the magnitude of EQTL events, and m_L satisfies $m_L = 1.29M - 5.65$, where M is the earthquake magnitude. The area-frequency curve of Luding EQTLs basically lay between the curves of $m_L = 3$ and $m_L = 4$ (Fig. 14), but the number of landslides with an area less than 200m² exceeded the upper bound of $m_L = 4$. It suggested that the frequency

of landslides with an area less than 200m² was higher than that of other EQTL events of similar magnitude.
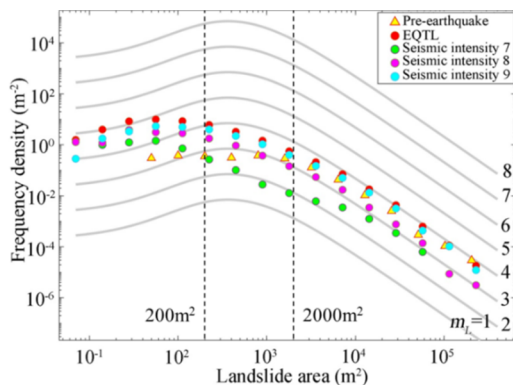
Fig. 14 Frequency-area curves of landslides pre-earthquake and earthquake-triggered landslides.

Compared with the landslide frequency-area curves from different seismic intensity areas, the EQTL frequency-area curve in the intensity VII area was under the curve of the whole landslide inventory, with a significantly lower level for landslides in the area of 100-10000m² in particular. The frequency-area curve in the intensity VIII area was between the curves of intensity VII and IX, and the value of the curve was slightly smaller than that of the curve in the intensity IX. The frequency-area curve in the intensity IX area was almost as same as the curve for all landslides.

By comparing the frequency-area curves of pre-earthquake landslides and EQTLs, significant difference between two landslide inventories was reflected in landslides with an area smaller than 2000m². The Luding earthquake induced a large number of landslides smaller than 2000m², and the frequency of these landslides was much higher than that of pre-earthquake landslides.

6.2 Post-Earthquake Geo-Hazards

6.2.1 Post-earthquake landslide

Since the earthquake destroyed the stability of slopes, meanwhile formed a large number of cracks, these unstable slopes were very prone to destabilization, therefore triggering new landslides because of rainfalls after the earthquake. Take the 2008 Wenchuan earthquake as an example. Compared to the landslide activity pre-earthquake, the landslide activity increased by 120 times in a short period of time after the earthquake, but decayed rapidly within 3 years after the earthquake and

basically returned to the pre-earthquake level within 10 years after the earthquake (Fan et al. 2019). Another study simulated rainfall-triggered landslides after the 2013 Lushan earthquake by using the SINMAP model, and found that the earthquake had a significant effect on the occurrence of rainfall-triggered landslides after the earthquake (Yang et al. 2015). Thus, post-earthquake rainfall-triggered landslides will become active during the rainy season of the year following the Luding earthquake.

6.2.2 Post-earthquake debris flows

After the earthquake, debris flows may become a more significant secondary hazard, which may be more extensive and active for a longer duration (Lan et al. 2013; Cui et al. 2014). According to the studies on debris flow in Wenchuan and Lushan earthquake-stricken areas, EQTLs located on slopes within small watersheds severely damaged the vegetation cover and changed the hydrological process in the watersheds. In the meantime, EQTLs also provided a large amount of loose solid mass for the debris flows. Such mass could be transported to gullies due to heavy rainfalls, thus forming new debris flows.

Regions that were strongly affected by the Luding EQTLs, such as Moxi town, Detuo town, Tianwan town and Caoke town, were exposed to active debris flows even before the earthquake. There were 32 debris flow watersheds that were severely affected by the EQTLs. Landslides provided large amount of sources in these watershed, which would intensify the activity and scale of these debris flows (Fig. 15). For example, located near Wandong Village, the Feishui gully with an area of 29.16km² had 510 EQTLs occurred in the watershed. The area of EQTLs covered 4.31 km², accounting for 14.78% of the watershed area (Fig. 16). In addition, debris flow gullies along the Tianwan River on the west side of the Xianshuihe fault, were also seriously affected by EQTLs, especially for the gullies on the left side of the river. Due to the increase of solid materials caused by EQTLs, some small watersheds also transformed into potential debris flow gullies, where debris flow would occur during the rainy season. Also, hillslope debris flow could become extremely active in the Luding earthquake-stricken area.

7 Conclusions

By comparing pre- and post-earthquake high-
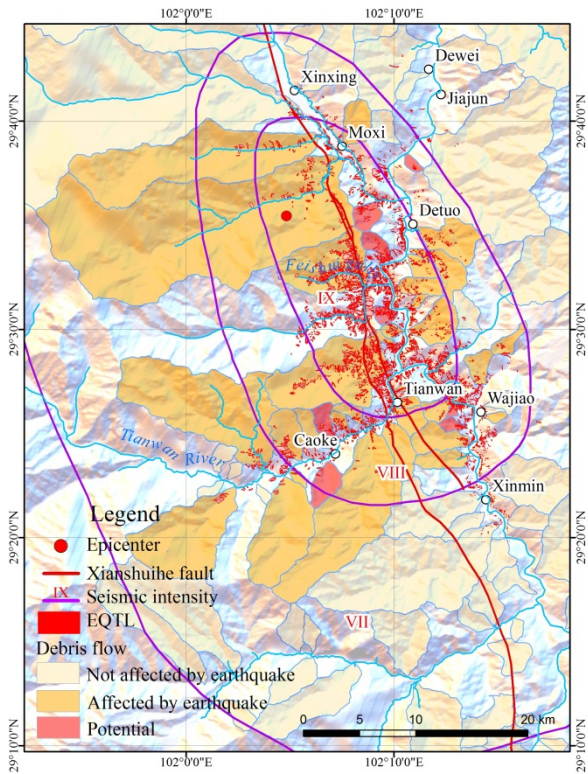
Fig. 15 Distribution of debris flow in Luding earthquake-stricken area.
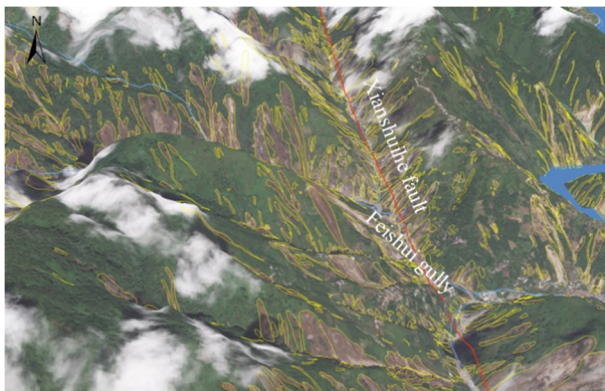
Fig. 16 Earthquake-triggered landslides in the Feishui gully.

resolution remote sensing images as well as the field investigation and validation of EQTLs, this study had a detailed inventory of landslides triggered by the M_S 6.8 Luding earthquake on September 5, 2022. A total of 8685 landslides were interpreted, with a whole area of 30.7km². The source area of the landslides was 9.4km², and the landslide-affected area was 760km². Luding EQTLs were mainly distributed in areas with an earthquake intensity of IX and VIII, accounting for 66.7% and 28.2%, respectively. A small portion of landslides also occurred in the areas with earthquake intensity VII.

Luding EQTLs were small and medium in size, which were mainly shallow landslides, and the thickness was generally 3-5m. Three main types of EQTLs were found: landslide, rockfall and slump. The landslide area of Luding EQTLs decreased with increasing distance from the Xianshuihe fault, which showed some patterns of dense distribution along the Xianshuihe fault, the river and the road. Luding EQTLs were mostly located near the foot of the slope, accounting for 47% of the total number of the landslides.

There was a power function relationship between the source area and the full area of landslides, as well as between landslide area and runout length. The relationship between the maximum slope of the landslide and the runout length showed that the larger the maximum slope of the landslide, the farther the runout length. With the increase of the runout length, the runout length was mainly influenced by the size of the landslide.

It is important to pay close attention to the slopes and debris flow gullies that were seriously affected by EQTLs in the Luding earthquake-stricken area. Risk assessment should be carried out on post-earthquake geo-hazards. Monitoring and early warning systems should also be deployed to high potential hazardous spots, so as to better support the rehabilitation and reconstruction in the Luding earthquake-stricken area.

Acknowledgments

Electronic supplementary material: Supplementary material (Appendix 1) is available in the online version of this article at https://doi.org/10.1007/s11629-022-7772-0.

References

Cui P, Wei FQ, He SM, et al. (2008) Mountain disasters induced by the earthquake of May 12 in Wenchuan and the disasters mitigation. Mt Res 26(3):280-282. (In Chinese) https://doi.org/10.3969/j.issn.1008-2786.2008.03.006

Cui P, Zhang JQ, Yang ZJ, et al. (2014) Activity and distribution of geohazards induced by the Lushan earthquake, April 20, 2013. Nat Hazards 73(2):711-726. https://doi.org/10.1007/s11069-014-1100-0

Dai F, Xu C, Yao X, et al. (2011) Spatial distribution of landslides triggered by the 2008 Ms 8.0 Wenchuan Earthquake, China. J Asian Earth Sci 40(4): 883-895. https://doi.org/ 10.1016/j.jseaes.2010.04.010

Fan X, Scaringi G, Korup O, et al. (2019) Earthquake-Induced Chains of Geologic Hazards: Patterns, Mechanisms, and Impacts. Rev Geophys 57(2): 421-503. https://doi.org/ 10.1029/2018RG000626

Fan X, Wang X, Dai L, et al. (2022) Characteristics and spatial distribution pattern of Ms 6.8 Luding earthquake occurred on September 5, 2022. J Eng Geol 30(5): 1504-1516. (In Chinese) https://doi.org/ 10.13544/j.cnki.jeg.2022-0665

Guo D, Hamada M, He C, et al. (2014) An empirical model for landslide travel distance prediction in Wenchuan earthquake area. Landslides 11(2):281–291. https://doi.org/10.1007/s10346-013-0444-y

Guzzetti F, Mondini AC, Cardinali M, et al. (2012) Landslide inventory maps: New tools for an old problem. Earth-sci Rev 112(1-2): 42-66. https://doi.org/10.1016/j.earscirev.2012.02.001

Harp EL, Jibson RW (1996) Landslides triggered by the 1994 Northridge, California, Earthquake. B Seismol Soc Am 86(1B): S319-S332.https://doi.org/10.3133/ofr95213

Hungr O, Leroueil S, Picarelli L (2014) The Varnes classification of landslide types, an update. Landslides 11(2):167–194. https://doi.org/10.1007/s10346-013-0436-y

Jibson RW, Harp EL, Keefer DK, et al. (1994) Landslides triggered by the Northridge Earthquake. Earthq Volcanoes 25(1): 31-41.

Qi S, Xu Q, Lan H, et al. (2010). Spatial distribution analysis of landslides triggered by 2008.5. 12 Wenchuan Earthquake, China. Eng Geol 116(1-2), 95-108. https://doi.org/10.1016/j.enggeo.2010.07.011

Keefer DK (1984) Landslides caused by earthquakes. Geol Soc Am Bull 95(4): 406-421.

Keefer DK, Wartman J, Navarro OC, et al. (2006) Landslides caused by the M 7.6 Tecomán, Mexico earthquake of January 21, 2003. Eng Geol 86(2–3): 183-197. https://doi.org/10.1016/j.enggeo.2006.02.017

Lan HX, Li L, Zhang YS, et al.(2013) Risk assessment of debris flow in Yushu seismic area in China: a perspective for the reconstruction. Nat Hazard Earth Sys 13(11), 2957-2968. https://doi.org/10.5194/nhess-13-2957-2013

Lee KL, Marcuson WF, Stokoe KH, et al. (1977) Research Needs and Priorities for Geotechnical Earthquake Engineering Applications, Report of Workshop at University of Texas, Austin, National Science Foundation Grant No. AEN77-09861. https:// doi.org/10.1016/0148-9062(79)90203-1

Li CY, Wang XC, He CZ, et al. (2019) China National Digital Geological Map (Public Version at 1:200,000 Scale) Spatial Database. Geol China 46(S1):1–14. (In Chinese)

Ling SX, Sun CW, Li XN, et al. (2021) Characterizing the distribution pattern and geologic and geomorphic controls on earthquake-triggered landslide occurrence during the 2017 M(s) 7.0 Jiuzhaigou earthquake, Sichuan, China. Landslides 18(4): 1275-1291.https://doi.org/10.1007/s10346-020-01573-6

Malamud BD, Turcotte DL, Guzzetti F, et al.(2004) Landslide inventories and their statistical properties. Earth Surf Proc Land 29(6):687-711. https://doi.org/10.1002/(ISSN)1096-9837

Meunier P, Hovius N, Haines JA (2008) Topographic site effects and the location of earthquake induced landslides. Earth Planet Sc Lett 275(3–4):221-232.

https://doi.org/10.1016/j.epsl.2008.07.020

Regmi AD, Dhital M R, Zhang JQ, et al. (2016) Landslide susceptibility assessment of the region affected by the 25 April 2015 Gorkha earthquake of Nepal. J Mt Sci 13(11):1941-1957. https://doi.org/10.1007/s11629-015-3688-2

Roback K, Clark MC, West AJ, et al. (2018) The size, distribution, and mobility of landslides caused by the 2015 M(w) 7.8 Gorkha earthquake, Nepal. Geomorphology 301(1): 121-138. https://doi.org/10.1016/j.geomorph.2017.01.030

Rodríguez CE, Bommer JJ, Chandler RJ (1999) Earthquake-induced landslides: 1980-1997. Soil Dyn Earthq Eng 18(5): 325-346.https://doi.org/10.1016/S0267-7261(99)00012-3

Su FH, Cui P, Zhang JQ, et al. (2013) Rockfall and landside susceptibility assessment in Lushan earthquake region. Mt Res 31(4):502-509. (In Chinese)

Tie YB, Zhang XZ, Lu JY, et al. (2022) Geo-hazards induced by Ms 6.8 Luding earthquake and mitigation. Hydrogeol Eng Geol 49(6): 1-12. (In Chinese) https:// doi.org/10.16030/j.cnki.issn.1000-3665.202209023

Varnes DJ (1954) Landslide types and processes. In: Eckel EB (ed) Landslides and engineering practice, special report 28. Highway research board. National Academy of Sciences, Washington, DC, pp 20–47.

Varnes DJ (1978) Slope movement types and processes. In: Schuster RL, Krizek RJ (eds) Landslides, analysis and control, special report 176: Transportation research board, National Academy of Sciences, Washington, DC, pp. 11–33.

Wang WN, Wu HL, Nakamura H, et al. (2003) Mass movements caused by recent tectonic activity: The 1999 Chi-Chi Earthquake in central Taiwan. Isl Arc 12(4): 325-334. https://doi.org/10.1046/j.1440-1738.2003.00400.x

Wu PP, Wang Y, Zhu J, et al. (2016) The characteristics of seismic activity on Xianshuihe fault since 1970 and the preliminary study on seismogenesis of the Kangding Ms6.3 earthquake. Earthq Res China 32(4):776-786. (In Chinese)

Xu C (2012) Detailed inventory of landslides triggered by the 2008 Wenchuan earthquake and its comparison with other earthquake events in the world. Sci Technol Rev 30(25):18-26. (In Chinese) https:// doi.org/10.3981/j.issn.1000-7857.2012.25.001

Xu C, Xu XW, Yu GH (2012) Landslides triggered by slipping - fault -generated earthquake on a plateau: An example of the 14 April 2010, Ms7.1, Yushu, China earthquake. Landslides 10:421-431.https:// doi.org/10.1007/s10346-012-0340-x

Xu X, Liu J, Zhang S, et al. (2018) Multi-period land use land cover remote sensing monitoring dataset in China (CNLUCC). Resource and Environmental Science Data Registration and Publication System. https://doi.org/10.12078/2018070201

Yang C, Zhang J, Zhang M (2013) A prediction model for horizontal run-out distance of landslides triggered by Wenchuan earthquake. Earthq Eng Eng Vib 12(2): 201-208. https://doi.org/10.1007/s11803-013-0163-3

Yang ZH, Lan HX, Liu HJ, et al. (2015) Post-earthquake rainfall-triggered slope stability analysis in the Lushan area. J Mt Sci 12(1): 232-242. https://doi.org/10.1007/10.1007/s11629-013-2839-6

Zhang JQ, Su FH, Fan JR (2013) Distribution of landslides and collapses induced by 2013 "4·20" Lushan earthquake and hazards assessment: a case study of S210 highway. Mt Res 31(5): 616-623. (In Chinese)

Zhao B (2021) Landslides triggered by the 2018 Mw 7.5 Palu supershear earthquake in Indonesia. Eng Geol 294: 106406. https://doi.org/10.1016/j.enggeo.2021.106406

Zhuang J, Peng J, Xu C, et al. (2018) Distribution and characteristics of loess landslides triggered by the 1920 Haiyuan Earthquake, Northwest of China. Geomorphology 314:1-12.https://doi.org/10.1016/j.geomorph.2018.04.012

Zhong C, Liu Y, Gao P, et al. (2020) Landslide mapping with remote sensing: challenges and opportunities. Int J Remote Sens 41(4): 1555-1581. https://doi.org/10.1080/01431161.2019.1672904